THE ELECTRONIC EFFECTS OF CD ON THE FORMATION OF THE CDS/CUINS$_2$ HETEROJUNCTION

B. JOHNSON, J. KLAER, A. VOLLMER, I. LAUERMANN

HELMHOLTZ-ZENTRUM BERLIN, ALBERT-EINSTEIN-STR. 15 12489 BERLIN, GERMANY

1. Abstract

The possibility of doping and Fermi Level pinning of $CuInS_2$ thin layer solar cell absorbers caused by the diffusion of Cd into the absorber during junction formation via chemical bath deposition was investigated. The analysis of thin CdS layers deposited on $CuInS_2$ showed the amount of deposition-induced band bending on the $CuInS_2$ surface (position of the Fermi Level in the respective band gaps) was not experimentally reproducible. However, the value of the valence band offset between the two materials was reproducible between different depositions within the error of the measurement. Thus, the deposition of the CdS does not lead to a consistent pinning position of the Fermi Level in the $CuInS_2$/CdS heterojunction. The removal of the CdS layers with HCl left a thin Cd-containing layer on the $CuInS_2$ surface and it was shown that this surface was not doped by the remaining Cd. Furthermore, the influence of the HCl of the $CuInS_2$ was explored and found to form a reproducible surface richer in Cu than $CuInS_2$ etched in potassium cyanide solution.

2. Introduction

Cu(In,Ga)S_2 (CIGS) is a promising absorber material for thin layer solar cells having the structure n^+-ZnO/i-ZnO/CdS/absorber/Mo/glass. With efficiencies reaching almost 13% this technology has already found its place in the PV market [1, 2], although the efficiency can be highly dependent on the method of production [3, 4, 5]. Although laboratory scale CIGS cells can have open circuit voltages above 800 meV, higher than similar cells from the low band gap selenide-absorber system (Cu(In,Ga)Se_2), the sulfide-based cells cannot produce a V_{oc} corresponding to their 1.6 eV band gap [2, 6]. This is also the case for the simpler $CuInS_2$ (CIS) system and its 1.5 eV band gap and V_{oc} of ~750 meV [5, 6]. The result is that

the selenide-based cells far out perform their sulfide-based counterparts in efficiency [7].

The junction between the CIS absorber and the CdS buffer layer is an extremely critical point of the solar cell and is not yet fully understood. In contrast to Cu(In,Ga)Se_2-based solar cells which are often described as having a spike alignment between the conduction bands of the absorber and the CdS buffer layer (absorber conduction band nearer to the Fermi Level than the buffer conduction band) [8], the conduction band alignment between the absorber and buffer layer in the sulfide-based solar cells is thought to be a cliff when analyzing solar cell grade materials (absorber conduction band further from the Fermi Level than the buffer conduction band) [9, 10, 11]. The cliff leads to increased interface charge carrier recombination because the Fermi-Level is at mid-band gap at the interface, allowing for relatively large hole and electron populations in a region of high defect density [8, 12]. The consequences of a non-optimized conduction band alignment can be alleviated somewhat if the absorber surface is inverted at the interface resulting in lower recombination velocities of photo-generated minority charge carriers which become majority charge carriers at the interface [8]. An inverted absorber surface in a semiconductor junction can be achieved in several ways. These include doping of the absorber surface via diffusion of an element from one layer into the other or interface states with proper charge pinning the Fermi-Level [13].

In this cell, the p-material is the CIS absorber itself, while the corresponding n-type material is the CdS. The p-n junction must, therefore, exist in the immediate vicinity of the CIS/CdS metallurgical junction, otherwise one would see large decreases in the short-circuit current density, j_{sc} [14]. It is not known, however, exactly where the p-n junction is located in this cell. One possibility is that Cd diffuses into the CIS and causes a type-inversion of the absorber surface from p to n-type which is present in the finished solar cell [15, 16, 17, 18] or that the intrinsic band bending on the CIS surface is increased by the deposition of the CdS through a pinning mechanism caused by band gap states created during deposition [13]. In this case the buried p-n junction would actually be a *homo*-p-n junction as opposed to the normally discussed “heterojunction” used to describe both the metallurgical and p-n junctions in this solar cell. Therefore, it is the goal of this investigation to determine whether

the Cd which is on the CIS surface or has diffused a short distance into the CIS results in an inverted CIS surface caused by pinning or doping.

Apart from the optimization of electronic positions on either side of the CIS/CdS interface, the open circuit voltage of a solar cell is first and foremost determined by the splitting of the quasi-Fermi Levels in the absorber which is, in turn, limited by the total amount of band bending in the space charge region [19]. This is also referred to as the built-in potential, V_{bi}. One can see then, why the enlarged band gap, E$_g$, should increase V_{oc} because the total amount of band bending cannot exceed the band gap E_g [20]. Thus, in the limit $T \rightarrow 0°C$ we have

$$V_{oc} \lesssim \frac{E_g}{q} \tag{1}$$

although in real solar cells at working temperatures a more realistic rule of thumb is [21]:

$$V_{oc} \sim \frac{2}{3}\frac{E_g}{q} \tag{2}$$

and we should expect a V_{oc} of at least 1000 mV from the CuInS$_2$-based solar cell ($E_g = 1.5\,eV$) instead of ~750 mV [5].

In this investigation, initial measurements on the CIS/CdS heterojunction to determine the valence band offset, ΔE_{vb}, resulted in constant values while the measured binding energies of the bands was not reproducible. When considering samples made with the same chemical bath (the shortest deposition times were 40 sec corresponding to a layer thickness of less than a nm) the measured position of the Fermi Level in the CIS and CdS band gaps which corresponds to the total amount of band bending on the CIS surface was often, but not always, the same and was largely independent of deposition time. Furthermore, there

seemed to be no correspondence between Fermi Level positions in samples stemming from different chemical baths. This suggests conclusions about the ability of the Cd to dope or pin the CIS surface and also means that the position of the Fermi Level in the CIS and CdS band gaps may depend not only on the actual CdS deposition but also on the measurement method, XPS and UPS, if they cause a surface photovoltage in samples with CdS [22, 23, 24].

In addition, the effect of the HCl etching on the CIS absorber surface which was often used during sample preparation is also considered.

3. Experimental

In order to remove the CuS_{2-x} secondary phases on the surfaces of all CIS samples formed as a consequence the layer production method, the absorbers were etched in 5% aqueous potassium cyanide (KCN) solution for three minutes before further treatment, including those used as references.

The CdS buffer layers were then deposited via chemical bath deposition (CBD) onto several different CIS absorbers grown by rapid thermal processing (RTP) [5]. The CBD was performed at 60°C for varying times and followed a standard recipe of 15 mL of 0.0165M Cd acetate dihydrate ($Cd(C_2H_3O_2)_2 \bullet 2H_2O$) in 25% NH_3 solution and 0.372M thiourea (H_2NCSNH_2) in 100 mL water. These were deposited into a double-walled glass container and filled to a final volume of 200 mL which led to final concentrations of 0.0012M Cd acetate dihydrate and 0.186M thiourea. The CIS absorbers were then dipped into the solution and left for varying times in order to obtain the desired thicknesses which are noted with each sample. After preparation the samples were transported in Ar to the UHV chamber. Contact with air ~~was~~ not avoided, although we attempted to limit this through the use of the inert gas.

After performing band offset measurements with X-ray and ultraviolet photoelectron spectroscopy (XPS, UPS) as described in [11, 25, 26], the CdS layers were removed through etching in 8% HCl. This process removed the entire CdS layer and left a Cd-containg layer on

the CIS surface which will be referred to as CIS:Cd [27, 28]. After HCl etching the samples were measured anew with XPS and UPS. Thus, it was possible to determine the difference in positions of the valence band and Fermi Level on the CIS surface both in the CIS/CdS junction and after CdS removal.

In addition, the stoichiometry and phase of the sample surfaces were investigated with XPS, UPS and Near-edge X-ray Absorption Spectroscopy (NEXAFS). The errors in both the UPS valence band edge measurements, which were evaluated by linearly extrapolating the band edge to the background, and the XPS core level binding energy measurements are ±0.10 eV. Errors of other measurements are noted in the text. The quantitative XPS measurements were calculated by integrating the measured peaks after background removal and normalizing by the number of scans, ionization cross-section [29], photoelectron mean free path [30] and the transmission function of the electron analyzer [31]. XPS core level binding energies are with reference to Au $4f_{7/2}$ at 83.8 eV and UPS valence bands with reference to the Fermi Level determined with freshly Ar-sputtered Au.

4. Results and Discussion

Chemical Bath Deposition-Induced Band Bending and Fermi Level Pinning

Fig. 1 shows UPS valence band spectra of several CIS samples after CdS depositions of duration 40 sec, 1 min, 2 min and 7 min, corresponding to layer thicknesses of about 0.7, 1, 2.5 and 35 nm, respectively, determined using the Lambert-Beer Law for absorption in matter. The electron absorption length was obtained from the reciprocal value of the electron mean free path (1.76 nm) calculated using the program Quases-Tourgaard [30] for electrons in CdS with a kinetic energy of 844 eV and corresponds to the Cd $3d_{5/2}$ core level excited with Mg Kα radiation. The layer thicknesses must be viewed as averages when considering the rough morphology of the CIS surface [32]. All CdS layers were made using different chemical baths. The samples have different CdS thicknesses and the same samples were later etched in HCl as it was of interest whether CdS deposition time had any effect on the CIS surface after

CdS removal.

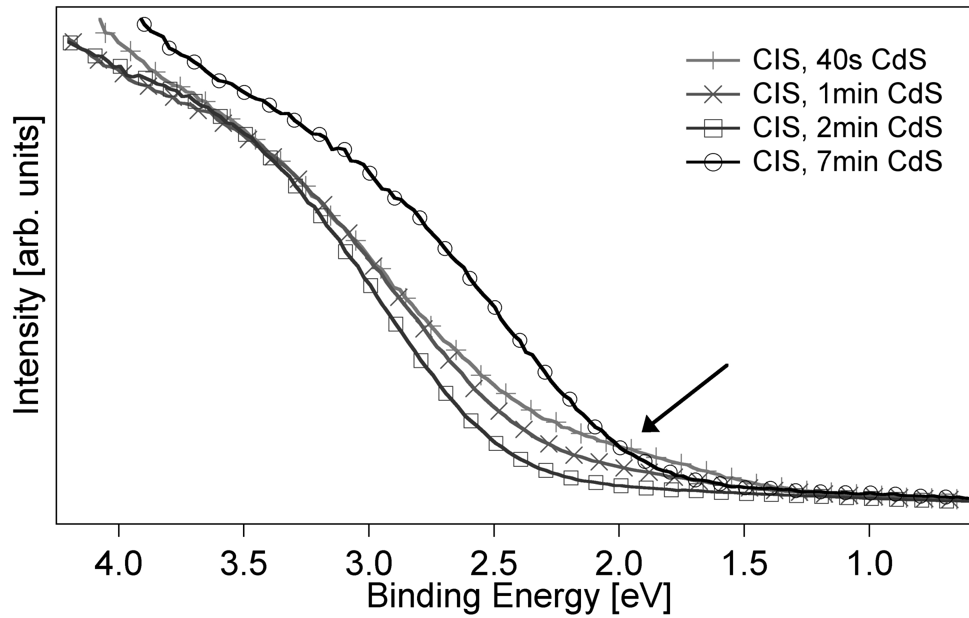

Figure 1: He I UPS valence band spectra of CdS on CIS substrates from different chemical bath depositions. The non-reproducibility of the positions of the band edges can be clarified through differing amounts of band bending on the underlying CIS surface.

The CdS spectra have each been multiplied by a separate factor in order to compare the measurements in a single figure, especially in the energy range 1.5-3.5 eV. In this region all spectra have a similar appearance apart from a decrease in signal intensity with deposition time at binding energies below the valence band edge. This corresponds to energies between about 1.5 and 2.5 eV and is denoted by a black arrow in the figure. The change is due to increasing CdS layer thickness leading to increased absorption and, therefore, attenuation of the signal from the underlying CIS. Also noticeable are the different positions of the band edges which can be clarified through differing amounts of band bending on the CIS surface occurring in different CdS depositions: a change in the amount of band bending on the CIS surface corresponds to a change in the Fermi Level position in the CIS band gap and also in the CdS band gap. This can be ascertained because no band bending in the CdS layer was observed with increased deposition time and the valence band offset, ΔE_{vb}, is constant as will be shown later. However, we note here that we found no correlation of this effect when

studying the secondary electron edge from the UPS measurements.

The band bending can be seen indirectly with XPS through a change in the CIS and CdS core level energies and the assumption that the energy difference between the valence band edge and the core levels of the substrate is fixed. There is no correspondence between the valence band position and CdS deposition time and will be discussed further below as part of the results of this experiment.

The samples with the 0.7 nm and 1 nm CdS layers have valence band edges at 2.20 eV and 2.25 eV, respectively, while the other two samples are shifted noticeably away from these values. The sample with 2.5 nm CdS layer has a band edge at 2.45 eV and the sample with 35 nm CdS, the thickest layer, is at 1.90 eV. By using the core levels measured on the CIS substrate before and after CdS deposition the additional band bending on the CIS surface can be ascertained and the band offset estimated with the equation

$$\Delta E_{vb} = E_{vb,CdS} - E_{vb,CIS} - E_{bb} \quad (3)$$

where the ΔE_{vb} is the valence band offset, $E_{vb,CdS}$ and $E_{vb,CIS}$ the measured positions of the valence band edges of CdS and CIS, respectively, and E_{bb} the change in core level binding energy on the CIS surface due to the additional CBD-induced band bending. We will assume in all cases that the valence band position of the CIS before the CdS is at $E_{vb,CIS}$=0.85 eV as measured on the KCN etched reference shown in the following section on doping. Although this is slightly higher than the normally observed value of $E_{vb,CIS}$=0.70-0.75 eV for CIS, it would add only 0.10 eV to the calculated band offset. This and another assumption that the valence band edge and core levels shift in parallel during CdS deposition are indeed critical and are discussed in [11], as well as references therein, along with other aspects of

this method.

For the samples with 0.7 nm, 1 nm and 2.5 nm CdS layer thicknesses the results for ΔE_{vb} in table 1 are found when the other values in the table are inserted into the corresponding terms in eq. 3.

Table 1: Measured values of the CdS and CIS valence band edges, $E_{vb,CdS}$, and $E_{vb,CIS}$, resepctively, as well as the band bending on the CIS surface induced by the CdS deposition, E_{bb}. The valence band offsets, ΔE_{vb}, calculated using eq. 3 are also presented.

Sample	$E_{vb,CdS}$ (eV)	$E_{vb,CIS}$ (eV)	E_{bb} (eV)	ΔE_{vb} (eV)
0.7 nm	2.20	0.85	0.15	1.20
1 nm	2.25	0.85	0.15	1.25
2.5 nm	2.45	0.85	0.40	1.20

The term E_{bb} was not only investigated by the CIS core levels, but also by looking at the positions of the Cd core levels in the different CdS layers. The correspondence between the shifts in Cd core levels and the Cu and In core levels supports band bending with the binding energies given in table 2. It must be noted that the core level shifts of Cu from the sample with the 2.5 nm CdS layer are smaller than expected. We cannot explain this deviation but believe it to be the result of a chemical shift in addition to band bending which has been seen in literature [33]. At the same time, the Cd 4d levels of this sample show a large shift with the direction supporting band bending. The results are supported by literature on solar cell quality CIS absorbers [9, 10, 11].

The sample with the 7:00 min CdS deposition time, at 35 nm layer thickness, was so thick that the underlying CIS core levels could no longer be measured and is, therefore, a little trickier to evaluate. However, if we look at the difference in Cd core levels between this sample and the other three samples (table 2) and compare them to the difference in the corresponding valence band edges, we find that although there is a small discrepancy the shifts are similar (table 3). All binding energies of the 35 nm sample were smaller than those of the other samples and such differences are defined here to be positive.

Table 2: Core level binding energies in eV from the KCN-etched sample and the samples after CdS deposition.

Core Level	KCN	0.7 nm CdS	1 nm CdS	2.5 nm CdS	35 nm CdS
Cu $2p_{3/2}$	931.05	931.20	931.20	931.15	
Cu $3p_{1/2}$	76.85	77.05	77.00	77.00	
Cu $3p_{3/2}$	74.40	74.55	74.55	74.60	
In $3d_{5/2}$	444.15	444.25	444.25	444.40	
In $3p_{3/2}$		665.35	665.30	665.50	
In $4d_{3/2}$	18.55	18.70	18.65	18.90	
In $4d_{5/2}$	17.65	17.80	17.80	18.05	
Cd $3d_{5/2}$		404.75	404.80	405.05	404.30
Cd $3p_{3/2}$		617.50	617.60	617.90	617.15
Cd $4d_{3/2}$		11.55	11.60	12.25	11.10
Cd $4d_{5/2}$		10.95	11.00	11.60	10.50

Table 3: Values for the differences between electronic positions of the sample with 35 nm CdS deposition time and the other three samples in fig. 1 as noted in the column on the left. The binding energies of the 35 nm sample were always smaller than those of the other samples. The differences in valence band positions are denoted by $\delta E_{vb} = E_{vb,CdS(x)} - E_{vb,CdS(35\,nm)}$, the differences in core level positions with $\delta E_{core} = E_{bb(x)} - E_{bb(35\,nm)}$ with $x = 0.7$ nm, 1 nm and 2.5 nm.

Sample	δE_{vb}	δE_{core}
0.7 nm	0.30 eV	0.40 eV
1 nm	0.35 eV	0.45 eV
2.5 nm	0.55 eV	0.80 eV

This parallel shift in levels again points to a shift in the position of the Fermi Level in the CIS band gap as seen in the other samples, although again, chemical shifts may be present. The sample with the thickest CdS layer, therefore, also follows the trend of a reproducible ΔE_{vb} and varying position of E_f.

Examining the values more closely, the position of the valence band edge of the thickest CdS layer, being at 1.90 eV, means that the valence band position on the CIS surface in this junction can be at a maximum of 0.70 eV in order to keep the 1.20 eV band offset, implying band bending *toward a more p-type surface* when compared to the value of 0.85 eV for the KCN-etched CIS reference found in fig. 4. This was the only observation of this trend in the present investigation. Of course, assuming a CIS valence band position of 0.85 eV on

this CIS surface (i.e. no deposition-induced band bending), the band offset of 1.05 is still inside of the error of these measurements of ±0.20 eV. This rather low value of ΔE_{vb} can be explained at least partially in terms of deposition times: this sample has the thickest CdS layer and we are comparing the electronic states on the CdS surface after 7 min of deposition time with those after 40 sec, 1 min and 2.5 min. Chemical shifts may be expected between these samples due to time dependent changes in concentrations in the chemical bath arising, for example, from the high vapor pressure and, therefore, continual loss of NH_3.

However, a more thorough explanation of the deviation of ΔE_{vb} and the binding energies of the 35 nm sample from those of the other samples can be obtained by considering other experimental details as well as surface photovoltage (SPV).

XPS has already been shown to cause an SPV, or charging, in samples containing a pn-junction [22, 23, 24] and, as can be seen in fig. 2, the same is the case in the CIS/CdS junction. An SPV is due to the creation of minority carriers in the space charge region which reduce the amount of band bending, exactly the same as in the solar cell under illumination [20]. In contrast to charging in XPS measurements where the sample is poorly contacted and leads to a depletion of negative charge and increased apparent binding energies of the electronic levels, the process here reduces the binding energy of the electrons through production of electron-hole pairs in the CIS. The hole population on the CIS surface, which was originally depleted (n-type surface, p-type bulk), increases under illumination and reduces the band bending and, therefore, the energy between the Fermi Level and the valence band edge. In fig. 2, XPS measurements at differing X-ray fluxes are shown for the Cd $3d_{5/2}$ core level from a ∼35 nm CdS layer deposited on CIS. This is not the same ∼35 nm sample as discussed above but the CdS deposition times and calculated thickness were equal. The total shift of just under 250 meV toward smaller binding energies caused by an SPV in the sample is evident between the highest and lowest incident fluxes which are loosely denoted by the photoelectron count rates.

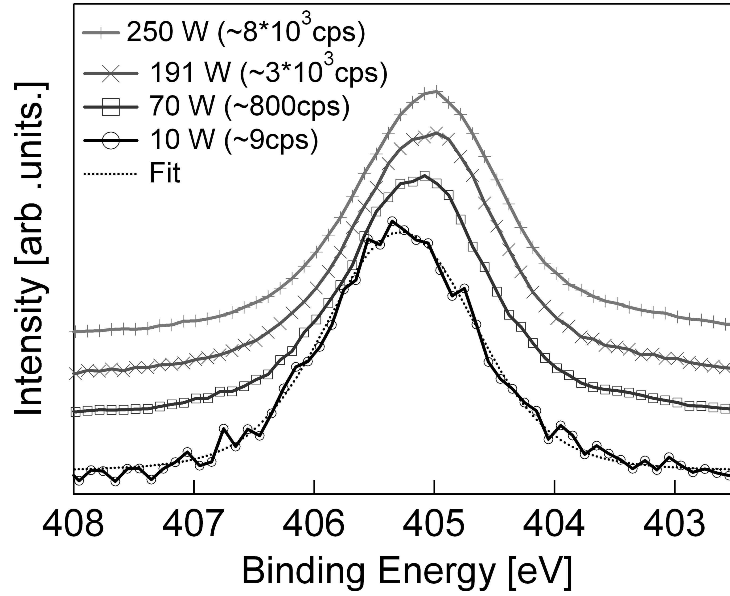

Figure 2: XPS measurements of the Cd 3d$_{5/2}$ core level from a ~35 nm CdS layer deposited on CIS at four different X-ray fluxes denoted by the photoelectron count rates. The total shift of ~250 meV caused by an SPV in the sample is evident between the measurements with the highest and lowest incident fluxes.

Fig. 3, on the other hand, shows the results of a similar measurement done on a CIS absorber with a ~1 nm CdS top-layer. This is a different ~1 nm sample than is discussed in the rest of the investigation. In this case it was possible to measure the Cd 3d$_{5/2}$ core level and the In 3d$_{5/2}$ core level from the substrate. Here there is a much smaller shift only noticeable in the measurement with the lowest incident flux. The shift of ~0.10 eV is less than the error of the measurement (±0.10 meV).

Similar experiments were conducted using UPS which covered about 2 orders of magnitude in photoelectron count rates. No dependence of the valence band position on intensity was observed although the UPS radiation contains a high amount of visible light. One reason for this is that any SPV caused by UV illumination is already present at incident photon fluxes much lower than those attainable with the UVS 10/35 UV source from Specs used in this investigation. The lowest power needed to ignite the plasma in the UV lamp produces a strong intensity in contrast to the XPS measurements which can be made at arbitrarily low incident photon fluxes. Other investigations of the valence bands measured with UPS and

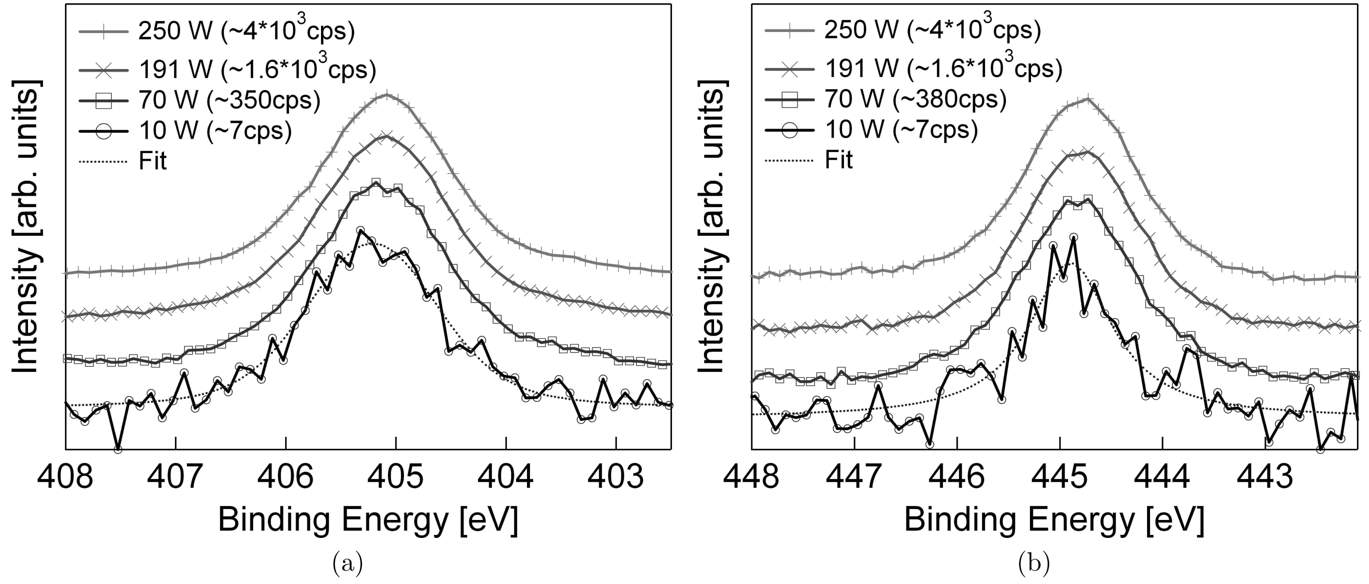

Figure 3: XPS measurements of the (a) Cd $3d_{5/2}$ and (b) In $3d_{5/2}$ core levels from a ∼1 nm CdS layer deposited on CIS at four different X-ray fluxes denoted by the photoelectron count rates. There is a minimal shift of ∼0.10 eV between the sample measured with the lowest incident flux and the other three.

XPS (not shown) indicate, furthermore, that at normal operation fluxes the resulting SPV in the CIS/CdS junction is higher with XPS.

The discrepancy between δE_{vb} and δE_{core} in table 3 can, then, be compensated for by considering charging effects caused by sample illumination. Beginning with the 2.7 nm and 35 nm samples, the difference between δE_{vb} and δE_{core} of 0.25 eV is nearly compensated for by the core level shifts in figs. 2 and 3, where the core levels of the thicker layer shows a nearly 0.2 eV shift over the thinner layer so that the valence band edges and core levels of these samples do indeed shift in parallel. If we assume that there is also an SPV present during the UPS measurements, larger in the thicker CdS sample than the thinner, this would clarify not only the difference in positions of the valence band edge but also the rather small ΔE_{vb} observed in the 35 nm sample or, alternatively, a CIS surface apparently becoming more p-type after junction formation.

Although the 0.7 nm and 1 nm samples are similar, the core levels in these samples are also shifted slightly due to an SPV during the XPS measurements and the discrepancy between δE_{vb} and δE_{core} in table 3 is, therefore, reduced to 0.10 eV. Looking at the valence band edges, there may be a small SPV due to the UV illumination in these two samples as well. The reason for considering the 2.5 nm CdS sample as being free of an SPV, at least in the UPS measurements, is that the valence band edge is at 2.45 eV which is equal to the band gap of the material. If this position was due to an SPV the CdS would be degenerate n-type in the dark.

The discrepancies in the band offset measurements and CBD-induced band bending on the CIS surface seem, then, to be a consequence of several factors related to both charging and to the CBD process. The measured binding energies in the junction are a result of the SPV induced in each junction during measurement and the SPV is dependent on the dynamic equilibrium which exists in each sample, i.e. on the rate at which the photo-generated charge carriers are swept out of the space charge region. Although most of the samples showing a large SPV similar to that of the 35 nm sample in fig. 1 had thick (>30 nm) CdS layers, this was not always the case: some measurements on samples with thick CdS top-layers led, without corrections for charging, to band offsets and absolute positions of the CdS valence band edge and core levels which were in agreement with measurements of samples with thinner layers. At the same time, thinner layers also occasionally showed small values of ΔE_{vb}, also presumably due to the SPV. Therefore, the dynamic equilibrium in each junction which leads to the SPV is not strictly dependent on layer thickness. This can be explained in terms of a thin interface layer between the CIS and CdS which is responsible, at least in part, for the rate at which the photo-generated charge carriers are removed from the space-charge region. This could be, for example, a consequence of the properties of the CIS surface after KCN etching immediately before CdS deposition leading to junctions with different properties or of the non-reproducibility of the chemical bath itself.

We conclude then that although the valence band offset between CIS and CdS is the same for every individual CdS deposition within experimental error, the Cd, or more generally, the

CdS deposition process, does not pin the Fermi Level at a specific electronic position on the CIS surface which is critical for solar cell functionality. If this were the case, the observed band bending on the CIS surface and, therefore, the position of the Fermi Level in the CdS, would be reproducible.

Cd as Dopant in $CuInS_2$

In fig. 4, the differences between the KCN-etched CIS reference layer and the other CIS layers after removal of the CdS can be clearly seen. The samples found in fig. 1 are also shown here, with the exception of the 35 nm sample, after the CdS layers were etched away with 8% HCl. The figure also contains a spectrum from an absorber etched in KCN and then in HCl without prior CdS deposition. The samples subjected to CdS deposition before the HCl etching contain a CIS:Cd layer on the surface as found in [27, 28]. The spectra have been normalized to enhance comparability between the individual valence band edges in the range 0.5-1.5 eV

In contrast to the KCN-etched CIS surface, the UPS measurements show the HCl etched surface to be highly reproducible. This is supported by the binding energies and surface stoichiometries measured with XPS on the same samples as will be discussed shortly. In addition to the samples discussed here, many other CIS absorbers etched with HCl after KCN etching had not only very similar valence band positions, 0.40 eV$< E_f - E_b <$0.50 eV, but also possessed valence bands whose entire forms were the same. This should be compared to the routinely seen spread in the measurements of the KCN-etched CIS samples: 0.55 eV$< E_f - E_b <$0.90 eV

The HCl-etched CIS surface shows a strong feature at 3 eV which is much weaker and at a slightly different energy in the spectra of the KCN-etched samples. These are the Cu 3d electrons, also visible in [26], here more prominent due to the increased Cu concentration on the CIS surface. Quantitative XPS measurements using Cu $2p_{3/2}$, In $3d_{5/2}$ and S 2p showed surface Cu-concentrations higher than on KCN-etched CIS. [Cu]/[In] ratios were routinely

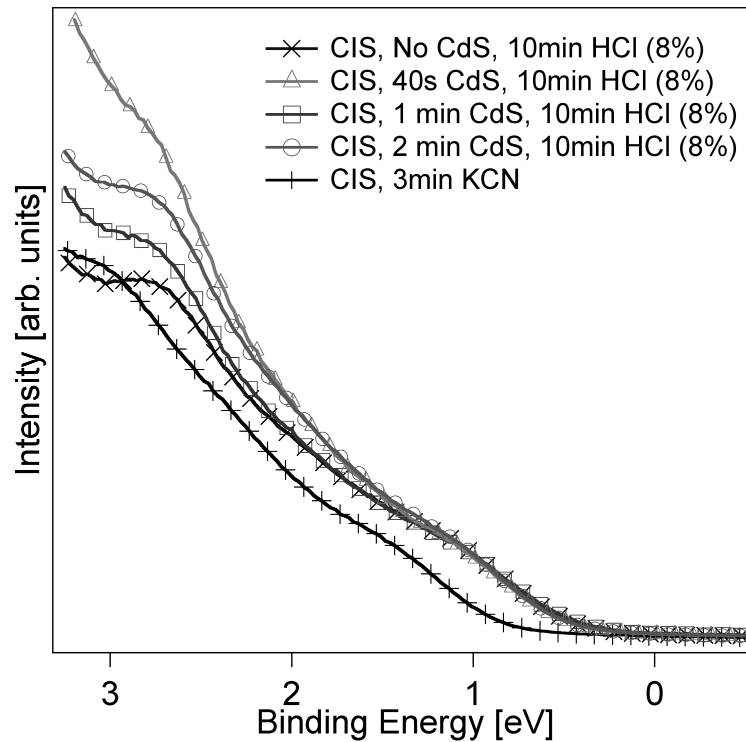

Figure 4: He I UPS valence band spectra of the same CIS absorbers found in fig. 1, without the 35 nm sample, after the removal of CdS with 8% HCl. Reference measurements are also shown from a KCN-etched as well as a KCN- and then HCl-etched (no CdS) absorber. The prominent Cu 3d peak at 3 eV is evidence for a Cu-richer surface after HCl etching.

between 0.53 and 0.62 for HCl-etched samples while this ratio was between 0.25 and 0.30 for KCN-etched samples. While the latter ratio is quite low, Cu-poor surfaces are also found in literature [34, 35, 36]. The amount of Cu therefore increased significantly after the HCl etching and, as discussed in [37, 38], the increased Cu concentration leads to an increased repulsion between the S 3p and Cu 3d states (p-d repulsion) and, therefore, to the shift of the valence band edge toward the Fermi Level. Due to contact with air we also considered the elemental ratios using the Cu 3p, In 4d and S 2p core levels. Their kinetic energies are similar making signal dampening from an adsorbate layer much less critical than with the core levels used above. These levels confirmed the trend of a Cu-richer surface after HCl etching with the [Cu]/[In] ratio for the KCN-etched sample increasing up to 0.35.

The observed change in stoichiometry can also be expected from the etching processes undertaken on the CIS layer. The first etch step in ~~amphoteric~~ KCN will remove oxides

from the sample surface and due to the strong ability of CN^- to form complexes, the Cu^+ will be preferentially removed from the surface, reflected in the Cu-poor CIS surface. In air the Cu-poor surface will form overwhelmingly indium oxides which will be removed by the subsequent HCl etch, leading to a Cu enrichment [39]. In addition, band bending can be likely ruled out as the main explanation for the shift in the position of the valence band edge after HCl etching by reviewing the core level positions between KCN and HCl etched CIS surfaces (table 4). Although a slight overall shift of core levels may be possible, it is not comparable to the shift in valence band edge of ~0.40 eV after the HCl-etch.

Table 4: Core level binding energies in eV from the KCN, KCN-HCl-KCN and KCN-HCl-etched sample surfaces

Core Level	KCN	KCN-HCl-KCN	HCl
Cu $2p_{3/2}$	931.05	931.15	931.10
Cu $3p_{1/2}$	76.85	76.85	76.80
Cu $3p_{3/2}$	74.40	74.40	74.35
In $3d_{5/2}$	444.15	444.10	444.05
In $3p_{3/2}$		655.15	665.10
In $4d_{3/2}$	18.55	18.45	18.35
In $4d_{5/2}$	17.65	17.60	17.50
S $2p_{1/2}$	162.60	162.55	162.55
S $2p_{3/2}$	161.40	161.35	161.30
S 2s	225.65	225.60	225.60

Because the forms of the valence bands and their edge positions are the same for HCl-etched samples with *and* without previous CdS deposition, the former containing a surface CIS:Cd layer, it is concluded that the Cd does not n-dope the CIS surface. In fact, the movement of the valence band edge toward E_f, when compared to KCN-etched samples, supports a more p-doped surface, although this is likely an effect of the Cu-richer HCl-etched surface.

The absence of any observed doping does not stand in contrast to Cd incorporating itself into the CIS lattice and forming a CIS:Cd surface. For example, one may alter the commonly discussed doping mechanism of Cd replacing Cu by also including the compensating effect of Cd occupying In lattice positions [40]. The effect of Cd on both lattice sites is also discussed

in [41].

Returning to the HCl-treated surfaces, [Cu 2p$_{3/2}$]/[S 2p] ratios determined with XPS also increased through the HCl etch step to between 0.25 and 0.33, compared with 0.18 for KCN-etched samples (or 0.25 when considering [Cu3p]/[S 2p]). This leads to the conclusion that In is preferably removed by HCl etching, at least at first, with perhaps some S following resulting in some phase of Cu$_{2-x}$S on the surface.

To investigate this, UPS valence band measurements were carried out in the following along with NEXAFS measurements which are very sensitive to some phases of CuS.

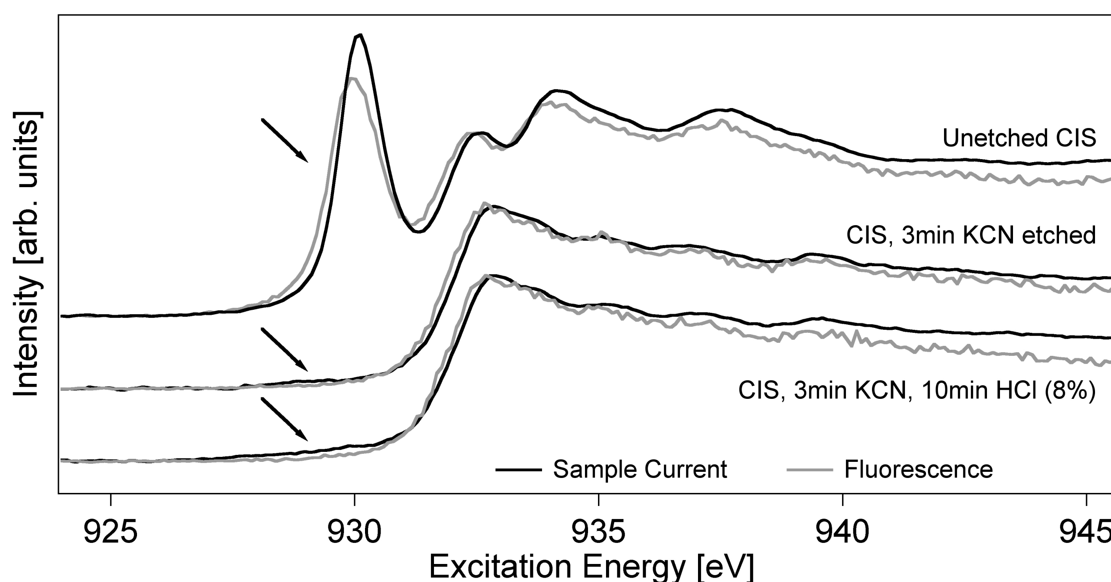

Figure 5: Cu L$_3$ absorption edges (blue is X-ray fluorescence, red is total electron yield) on unetched, KCN-etched and KCN-HCl-etched CIS samples. The large feature at 930 eV in the unetched spectrum (black arrow) is due to the CuS and CuO phases on the surface of the sample with a Cu 3d^{9}4s^0 valence structure. The HCl etching, although it produces a Cu-richer CIS surface than found on KCN-etched CIS, produces no phase with a Cu 3d^{9}4s^0 valence structure. The spectra are normalized to the peak at 932 eV following the pre-edge feature and are shifted vertically for clarity.

Fig. 5 shows several Cu L$_3$ absorption edges from unetched and KCN-etched absorbers as well as an absorber etched in KCN and then in HCl (KCN-HCl-etched). The very prominent pre-edge feature at 930 eV (black arrow) in the unetched sample is caused by the presence of

a phase with a partially empty Cu 3d orbital (Cu $3d^9 4s^0$) [42], the empty 3d state being in the conduction band. Even very small amounts of this phase on the surface can contribute a large pre-edge feature to the absorption spectrum due to the high oscillator strength between the Cu 2p and Cu 3d states. These phases can include any compound with Cu bound as Cu (II) such as Cu(II)O and some kinds of $Cu_{2-x}S$ where there is at least a partially open 3d orbital [42, 43].

Therefore, when looking at the other two spectra in fig. 5, it can be seen that neither the KCN-etched CIS nor the KCN-HCl-etched CIS contains any amount of this Cu $3d^9 4s^0$ phase on the surface in concentrations corresponding to anything but slight contaminations, probably from oxidation during sample transport and loading.

Several other features in the spectra in fig. 5 are noteworthy. The reduced and/or absent pre-edge feature at 930 eV in all three spectra with fluorescence signal can be explained by the different information depths of the two signals. The relatively bulk-sensitive nature of X-ray fluorescence detects proportionally less of the Cu(II)-containing phase compared to total electron yield because this phase is not present in the bulk of the absorber. Also, the slight deviation in the position of the absorption edges measured by fluorescence and total electron yield on each sample shows a slight change in the energy between the Cu 2p core level and the final state of the absorption event (Cu-d and -s states) when moving deeper into the sample bulk and supports the well-known concentration gradients found in solar cell-grade chalcopyrites [34, 35, 36].

Further investigation of the HCl-etched surface was performed with UPS valence band measurements of several samples.

Fig. 6 shows the valence band edges of an unetched CIS sample, a KCN-etched sample, a KCN-HCl-etched sample and a sample etched in KCN, then HCl and then again in KCN (KCN-HCl-KCN-etched). The spectra have been normalized for comparability of the main features. The unetched sample with presumably CuO, CuS and Cu_2S phases on the surface

clearly has a metallic nature as can be seen from the small Fermi Level at 0 eV (inset). In this spectrum as well, a somewhat washed-out Cu 3d feature is visible at 3 eV. While $Cu_{2-x}S$ is known to be metallic for some values of x [44, 45], the resistivity values can vary over several orders of magnitude and depend on the purity of the material. Metallicity is, therefore, not a direct criterion for the existence of $Cu_{2-x}S$ with specific x values. Additionally, the problem of ascertaining the value of x is exacerbated because the $Cu_{2-x}S$ phase is on a $CuInS_2$ substrate making it difficult to determine how much of the Cu and S signals come from the substrate and how much from the $Cu_{2-x}S$.

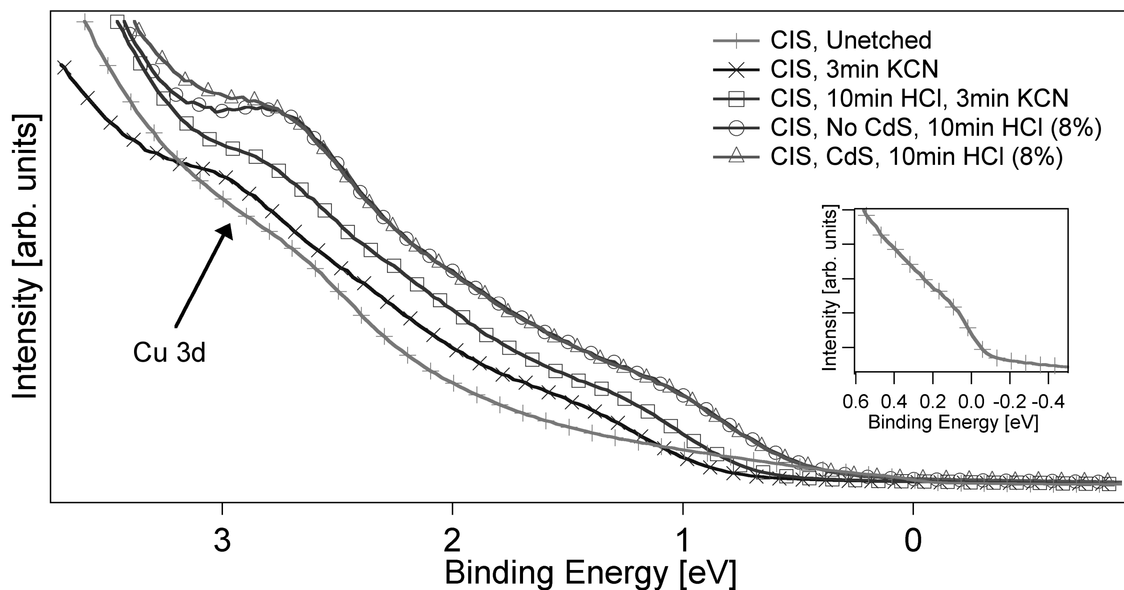

Figure 6: UPS valence band measurements of unetched, KCN-etched, KCN-HCl-etched and KCN-HCl-KCN-etched CIS absorbers. The metallic nature of the unetched sample can be clearly seen (Fermi Level, inset) as well as the effect of the KCN etching when it follows HCl etching. The measurement of the KCN-HCl-KCN sample lies between that of the KCN and KCN-HCl samples.

At the other extreme, having a valence band edge at 0.85 eV, is the valence band edge of a KCN-etched CIS absorber (this is the same spectrum as in fig. 4). As usual, the Cu 3d peak is rather weak and shifted to slightly higher binding energies due to the Cu-poorer surface.

In between these two extremes are spectra from samples etched in HCl, one after the removal of a CdS buffer layer which, therefore, contains a CIS:Cd surface layer, and one having

been subjected to no previous CdS deposition. The measurement on the KCN-HCl-KCN sample is also found here. It can immediately be seen, as in fig. 5, that the surface created by the HCl etch step is not the same as the unetched surface as the valence bands look very different. However, the valence band edge of the KCN-HCl-KCN-etched sample looks very similar to the valence band of the CIS sample etched only in KCN. If the Cu-rich phase produced by the HCl were indeed CuS, it must be removable by a further KCN etch step and the valence band should return to one similar to the KCN-etched sample as seen here.

The KCN-HCl-KCN sample has a valence band edge at 0.70 eV, very typical for KCN-etched CIS, and the Cu 3d peak at 3 eV is also very similar to that of KCN-etched CIS. Because the KCN-etched CIS sample measured here showed slightly anomalous values (see previous section), it is possible that after a subsequent HCl and KCN etch step, the surface does not return to its exact original form, but rather to one which is more representative of KCN-etched CIS in general.

Therefore, it seems that the HCl etching produces a nonmetallic $Cu_{2-x}S$ phase on the CIS surface with a closed d-shell because the pre-edge feature at 930 eV in fig. 5 is not found after HCl etching. A $Cu_{2-x}S$ phase is further supported by the valence band spectrum of the HCl-etched sample after a subsequent KCN etch step which returns to a form similar to that of a sample etched solely in KCN. This indicates a layered surface-near region of HCl-etched CIS, for example: $Cu_{2-x}S/CuInS_2$(Cu-richer)/$CuInS_2$(Cu-poorer).

A KCN, HCl and subsequent second KCN etch step may be a method to achieve reproducible CIS surfaces.

5. Conclusion

Analysis of the electronic structure of the $CuInS_2$/CdS heterojunction showed that although the valence band offset, ΔE_{vb}, has a value of 1.25 eV±0.20 eV in all samples, the measured energy between the Fermi Level and the CIS valence band edge, $E_f - E_{VB,CIS}$, on

the CIS surface after CdS deposition is not reproducible. This is due both to differences in the CdS CBD process as well as surface photovoltage effects caused by the XPS and UPS measurement methods themselves. After removal of the CdS layers with HCl etching, the electronic structure of the valence band of the CIS surfaces with and without a surface Cd layer are the same. Therefore, the CdS deposition does not pin the Fermi Level at a position in the CIS/CdS junction crucial to the functionality of the solar cell, nor does the Cd dope the CIS surface. These results support the importance of the n^+-ZnO window layer in determining the final band structure of the solar cell because the reproducibility of solar cell characteristics implies the similarity of band alignments in individual solar cells. Furthermore, although Cd is not responsible for an inverted absorber surface layer, inversion could still be achieved after application of the ZnO due to the intrinsic band bending present on the nearly inverted KCN-etched absorber surface. The HCl etching used in this study leads to a reproducible CIS surface which is Cu-richer than KCN-etched CIS surfaces, possibly the result of a CuS_{2-x} surface layer with a closed d-shell. A subsequent KCN etch returns the HCl-etched surface to one resembling a surface etched only in KCN.

6. Acknowledgements

Financial support was provided by the German Bundesminesterium für Umwelt, support code 0327589B (KD-CIS). I would also like to thank Ina Halfpap und Shivanand Bhure for their help in the Chemical and UHV Laboratories during the summer of 2010 as well as Prof. Dr. Christian Pettenkofer for providing much needed insight about the effects of surface photovoltage.

References

[1] N. Meyer, A. Meeder, D. Schmid, Thin Solid Films, **515**, 5979-5984 (2010)

[2] S. Merdes, R. Mainz, J. Klaer, A. Meeder, H. Rodriguez-Alvarez, H.W. Schock, M.Ch. Lux-Steiner, R. Klenk, Solar Energy Materials & Solar Cells, (2010), doi: 10.1016/j.solmat.2010.11.003

[3] S. Merdes, B. Johnson, R. Sáez-Araoz, A. Ennaoui, J. Klaer, I. Lauermann, R. Mainz, A. Meeder, R. Klenk, Current Transport in Cu(In,Ga)S_2 based solar cells with high open circuit voltage-bulk vs. inerface, Mater. Res. Soc. Symp. Proc. 1165-M05-15 (2009)

[4] I. Riedel, J. Riediger, J. Ohland, J. Keller, M. Knipper, J. Parisi, R. Mainz, S. Merdes, Solar Energy Materials & Solar Cells, **95**, 270-273 (2011)

[5] S. Siemer, J. Klaer, I. Luck, J. Bruns, R. Klenk, D. Bräunig, Solar Energy Materials and Solar Cells **67**, 159-166 (2001)

[6] R. Klenk, S. Bakehe, R. Kaigawa, A. Neisser, J. Reiß, M.Ch. Lux-Steiner, Thin Solid Films **451-452**, 424-429 (2004)

[7] C.A. Kaufmann, T. Unold, D. Abou-Ras, J. Bundesmann, A. Neisser, R. Klenk, R. Scheer, K. Sakurai, H.-W. Schock, Thin Solid Films, **515**, 6217-6221 (2007)

[8] R. Klenk, Thin Solid Films **387**, 135-140 (2001)

[9] R. Scheer, Trends in Vacuum Science and Technology **2**, 77-112 (1997)

[10] A. Klein, T. Löher, Y. Tomm, C. Pettenkoffer, W. Jaegermann, Appl. Phys. Lett. **70**, 1299-1301 (1997)

[11] B. Johnson, L. Korte, T. Lußky, J. Klaer, I. Lauermann, J. Appl. Phys. **106**, 073712 (2009)

[12] I. Hengel, A. Neisser, R. Klenk, M. Ch. Lux-Steiner, Thin Solid Films **361-362**, 458 (2000)

[13] J. Tersoff, Phys. Rev. B **30**, 4874-4877 (1984)

[14] P. Pistor, R. Klenk, Proceedings of NUMOS (Numerical Modelling of Thin Film Solar Cells), Gent, Belgium, pg. 28-30, (2007)

[15] K. Ramanathan, H. Wiesner, S. Asher, D. Niles, R. N. Battacharya, M. A. Contreras, R. Noufi, Proc. 2nd World Conf. Photovoltaic Solar Energy Conversion, 477 (1998)

[16] T. Wada, S. Hayashi, Y. Hashimoto, S. Nishiwaki, T. Sato, T. Negami, M. Nishitani, Proc. 2nd World Conf. Photovoltaic Solar Energy Conversion, 403 (1998)

[17] P. Fons, K. Sakurai, A. Yamada, K. Matsubara, K. Iwata, T. Baba, Y. Kimura, H. Nakanishi, S. Niki, J. Phys. Chem. Solids **64**, 1733-1735, (2003)

[18] D. Abou-Ras, G. Kostorz, A. Romeo, D. Rudmann, A. N. Tiwari, Thin Solid Films **480-481**, 118-123 (2005)

[19] W. Jaegermann, A. Klein, T. Mayer, Advance Materials, **21**, 4196-4206 (2009)

[20] S. J. Fonash, *Solar Cell Devices*, Academic Press, New York (1981)

[21] E. Miller, On Solar Hydrogen & Nanotechnology, L. Vayssieres, Ed, John Wiley & Sons (2009)

[22] W. Jägermann, C. Pettenkofer, B. A. Parkinson, Phys. Rev. B **42** 7487-7496 (1990)

[23] A. Schellenberger, R. Schlaf, C. Pettenkoffer, W. Jaegermann, Phys. Rev. B **45** 3538-3545 (1992)

[24] A. Schellenberger, Dissertation, Freie Universität zu Berlin (1992)

[25] Y. Hashimoto, K. Takeuchi, K. Ito, Appl. Phys. Lett. **67**, 980-982 (1995)

[26] L. Weinhardt, O. Fuchs, D. Groß, G. Storch, E. Umbach, N. G. Dhere, A. A. Kadam, S. S. Kulkarni, C. Heske, Appl. Phys. Lett. **86**, 062109-062111 (2005)

[27] B. Johnson, J. Klaer, Ch.-H. Fischer, I. Lauermann, Depth profiling of a CdS buffer layer on $CuInS_2$ measured with X-ray photoelectron spectroscopy during removal by HCl etching, Thin Solid Films (2011) doi:10.1016/j.tsf.2011.10.144

[28] A. Rockett, D. Liao, J. T. Heath, J. D. Cohen, Y. M. Strzhemechny, L. J. Brillson, K. Ramanathan, W. N. Shafarman, Thin Solid Films **431-432**, 301-306 (2003)

[29] M.B. Trzhaskovskaya, V.I. Nefedov, V.G. Yarzhemsky, Atomic Data and Nuclear Tables **77**, 97-159 (2001)

[30] S. Tanuma, C. J. Powell, D. R. Penn, Surf. Interf. Anal., **21**, 165 (1993)

[31] Practical Surface Analysis, D. Briggs, M. P. Seah, Ed., John Wiley & Sons, New York, New York, USA (1983)

[32] I. Luck, J. Kneisel, K. Siemer, J. Bruns, R. Scheer, R. Klenk, N. Janke, D. Bräunig, Solar Energy Materials and Solar Cells **67**, 151-158 (2001)

[33] N. G. Dhere, A. A. Kadam, A. H. Jahagirdar, S. S. Kulkarni, L. Weinhardt, D. Groß, C. Heske, E. Umbach, J. Phys. and Chem. of Solids **66**, 1872-1875 (2005)

[34] I. Lauermann, Ch. Loreck, A. Grimm, R. Klenk, H. Mönig, M. Ch. Lux-Steiner, Ch.-H. Fischer, S. Visbeck, T. P. Niesen, Thin Solid Films **515** 6015-6019 (2007)

[35] H. Mönig, Ch.-H. Fischer, R. Caballero, C.A. Kaufmann, N. Allsop, M. Gorgoi, R. Klenk, H.-W. Schock, S. Lehmann, M.C. Lux-Steiner, I. Lauermann, Acta Materialia, **57**, 3645-3651 (2009)

[36] K. Müller, R. Scheer, Y. Burkov, D. Schmeißer, Thin Solid Films, **451**, 120-123 (2004)

[37] J. E. Jaffe, A. Zunger, Phys. Rev. B **27**, 5822-5847 (1983)

[38] J. E. Jaffe, A. Zunger, Phys. Rev. B **28**, 5822-5847 (1983)

[39] CRC Handbook of Chemistry and Physics 67th Edition, R.C. Weast, Ed., CRC Press, Inc, Florida, USA (1986-87)

[40] H.-W. Schock, private communication, 2011

[41] D. Liao, A. Rockett, J. Appl. Phys. **93**, 9380-9382 (2003)

[42] M. Grioni, J.B. Goedkoop, R. Schoorl, F. M. F. de Groot, J.C. Fuggle, Phys. Rev. B **39**, 1541-1545 (1989)

[43] R. Bacewicz, A. Wolska, K. Lawniczak-Jablonska, Ph. Sainctavit, J. Phys.: Condens. Matter **12**, 7371-7379 (2000)

[44] K. Okamoto, S. Kawai, R. Kiriyama, Jap. J. Appl. Phys. **8**, 718-724 (1969)

[45] H. Nozaki, K. Shibata, N. Ohhashi, J. Solid State Chem. **91**, 306-311 1991

Figures

Fig. 1: He I UPS valence band spectra of CdS on CIS substrates from different chemical bath depositions. The non-reproducibility of the positions of the band edges can be clarified through differing amounts of band bending on the underlying CIS surface.

Fig. 2: XPS measurements of the Cd $3d_{5/2}$ core level from a ~35 nm CdS layer deposited on CIS at four different X-ray fluxes denoted by the photoelectron count rates. The total shift of ~250 meV caused by an SPV in the sample is evident between the measurements with the highest and lowest incident fluxes.

Fig. 3: XPS measurements of the (a) Cd $3d_{5/2}$ and (b) In $3d_{5/2}$ core levels from a ~1 nm CdS layer deposited on CIS at four different X-ray fluxes denoted by the photoelectron count rates. There is a minimal shift of ~0.10 eV between the sample measured with the lowest incident flux and the other three.

Fig. 4: He I UPS valence band spectra of the same CIS absorbers found in fig. 1, without the 7:00 min sample, after the removal of CdS with 8% HCl. Reference measurements are also shown from a KCN-etched as well as a KCN- and then HCl-etched (no CdS) absorber. The prominent Cu 3d peak at 3 eV is evidence for a Cu-richer surface after HCl etching.

Fig. 5: Cu L_3 absorption edges (blue is X-ray fluorescence, red is total electron yield) on unetched, KCN-etched and KCN-HCl-etched CIS samples. The large feature at 930 eV in the unetched spectrum (black arrow) is due to the CuS and CuO phases on the surface of the sample with a Cu $3d^9 4s^0$ valence structure. The HCl etching, although it produces a Cu-richer CIS surface than found on KCN-etched CIS, produces no phase with a Cu $3d^9 4s^0$ valence structure. The spectra are normalized to the peak at 932 eV following the pre-edge feature and are shifted vertically for clarity.

Fig. 6: UPS valence band measurements of unetched, KCN-etched, KCN-HCl-etched and

KCN-HCl-KCN-etched CIS absorbers. The metallic nature of the unetched sample can be clearly seen (Fermi Level, inset) as well as the effect of the KCN etching when it follows HCl etching. The measurement of the KCN-HCl-KCN sample lies between that of the KCN and KCN-HCl samples.